The Wave–Turbulence Transition for Stratified Flows

ERIC A. D'ASARO

Applied Physics Laboratory and School of Oceanography, University of Washington, Seattle, Washington

REN-CHIEH LIEN

Applied Physics Laboratory, University of Washington, Seattle, Washington

(Manuscript received 7 April 1999, in final form 11 August 1999)

ABSTRACT

Mixing in a stratified ocean is controlled by different physics, depending on the large-scale Richardson number. At high Richardson numbers, mixing is controlled by interactions between internal wave modes. At Richardson numbers of order 1, mixing is controlled by instabilities of the large-scale wave modes. A ''wave–turbulence'' (W–T) transition separates these two regimes. This paper investigates the W–T transition, using observed oceanic and atmospheric spectra and parameterizations. Viewed in terms of Lagrangian (intrinsic) frequency spectra, the transition occurs when the inertial subrange of turbulence, confined to frequencies greater than the buoyancy frequency N, reaches the level of the internal waves, confined to frequencies less than N. Viewed in terms of vertical wavenumber spectra, the W–T transition occurs when the bandwidth of internal waves becomes small. Both of these singularities occur when the typical internal wave velocity becomes comparable to the phase speed of the lowest internal wave mode. At energies below that of the W–T transition, the dissipation rate varies as the energy squared; above the transition the dependence is linear. The transition occurs at lower shear and dissipation rates where the phase speed of the lowest mode is smaller, that is, in shallower water for the same stratification. Traditional turbulence closure models, which ignore internal waves, can be accurate only at energies above the W–T transition.

1. Introduction

Two very different classes of models have been used to understand turbulence and mixing in stratified geophysical flows. One approach attempts to extrapolate the physics of unstratified turbulence into the stratified regime. Such ''stratified turbulence'' models (Mellor and Yamada 1982; Luyten et al. 1996) work well if the stratification is not too strong and the flow remains highly turbulent, but fail if the stratification is too strong (Simpson et al. 1996). A second approach attempts to extrapolate the physics of internal waves into a partially turbulent regime. Such ''wave–wave interaction'' models (Müller et al. 1986) work well in the weakly turbulent ocean thermocline (Gregg 1989; Polzin et al. 1995; Winkel 1998) but have not been well tested in other regimes. The two classes of models are fundamentally different in their physical assumptions and mathematical forms and will yield very different results if applied to the same flow.

The two different classes of models are designed to operate in different large-scale Richardson number regimes. Wave–wave interaction models assume that the flow can be expressed as the sum of interacting internal waves, each of which is a solution to the inviscid linear internal wave equations. Energy transfer and fluxes occur through the interactions of these waves. This approach is appropriate at high large-scale Richardson numbers, where the waves are stable and interact only weakly. Stratified-turbulence models generally parameterize fluxes by assuming a local turbulent eddy viscosity, or similar closure, whose strength depends on the local time and length scales of the flow. This approach is appropriate at low Richardson number where the flow is mostly turbulent and waves play only a minor role (Henyey 1989). A transition from the high Richardson number wave physics to the low Richardson number turbulent physics should occur at some intermediate Richardson number. We will call this the *wave* to *stratified turbulence transition*, or W–T transition. It is the focus of this paper.

We will study the W–T transition from an oceanographic viewpoint, considering how the physics of a broadband, high Richardson number flow, dominated by internal waves, such as that in the open ocean thermocline, changes as its energy increases. The analysis

Corresponding author address: Dr. Eric A. D'Asaro, Applied Physics Laboratory, School of Oceanography, University of Washington, 1013 NE 40th Street, Seattle, WA 98105.
E-mail: dasaro@apl.washington.edu.

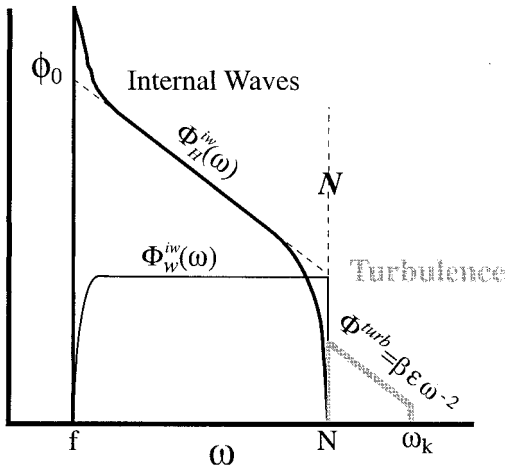

FIG. 1. Model Lagrangian frequency spectra of vertical [$\Phi_w(\omega)$] and horizontal [$\Phi_H(\omega)$] velocity as a function of Lagrangian frequency ω. The model consists of an internal wave component ($f < \omega < N$), extending from the Coriolis frequency f to the buoyancy frequency N, and a turbulent component ($N < \omega < \omega_k$), extending to the Kolmogorov frequency ω_k and proportional to the turbulent dissipation rate ε.

is based on the observed shapes of oceanic and atmospheric spectra and existing parameterizations of the dissipation rate. We first (section 2) consider the Lagrangian frequency spectrum of velocity, a recently measured quantity. We then (section 3) consider the Eulerian wavenumber spectrum of shear, a quantity that is well measured and modeled in the oceanic thermocline. Neither spectrum can maintain its low energy form at high energy, implying that a transition must occur. We then quantify the transition (section 4) and find that both spectra lose their low energy form at the energy level at which the rms velocity reaches approximately the lowest mode phase speed. We compare these predictions with oceanic observations and traditional turbulence closure models (section 5) and finally (section 6) summarize and discuss the limitations of the analysis.

2. Lagrangian frequency spectrum

Lien et al. (1998) and D'Asaro and Lien (2000) describe frequency spectra ($\Phi_u(\omega)$, $\Phi_v(\omega)$, $\Phi_w(\omega)$) [m^2 s^{-1}] of velocity (u, v, w) [m s^{-1}] as a function of Lagrangian frequency ω [s^{-1}], as observed by neutrally buoyant floats in regions of both strong and weak turbulence. On the basis of their observations, we propose the spectral form shown in Fig. 1. The model spectrum is the sum of internal wave and turbulent components.

Motions with $N > \omega > f$, where f is the Coriolus frequency, are modeled as internal waves. These satisfy the internal wave consistency relationship (Fofonoff 1969; Calman 1978)

$$\frac{\Phi_w^{\text{iw}}}{\Phi_H^{\text{iw}}} = \frac{\omega^2(\omega^2 - f^2)}{(N^2 - \omega^2)(\omega^2 + f^2)}, \tag{1}$$

where $\Phi_H^{\text{iw}} = \Phi_u^{\text{iw}} + \Phi_v^{\text{iw}}$. We model the internal wave horizontal velocity spectrum using a minor variant on GM76 (Gregg and Kunze 1991), a traditional combination of Garrett and Munk (1975) and Cairns and Williams (1976). The spectral form is

$$\Phi_H^{\text{iw}}(\omega) = \phi_0 \frac{f^2}{\omega(\omega^2 - f^2)^{1/2}} B(\omega), \tag{2}$$

where ϕ_0 is a constant that sets the internal wave energy and B describes the shape of the spectrum near N. For $N \gg \omega \gg f$, Φ_H^{iw} has a spectral slope of -2 and Φ_w^{iw} is white. Observed Φ_w sometimes show peaks near $\omega = N$. We will ignore these and choose

$$B(\omega) = (N^2 - \omega^2)/N^2 \tag{3}$$

so as to make Φ_w^{iw} white with a value of

$$\Phi_w^{\text{iw}} = \phi_0 \frac{f^2}{N^2} \tag{4}$$

for $f \ll \omega < N$.

Motions with $\omega > N$ are modeled as turbulence. We assume isotropic turbulence, $\Phi_H^{\text{turb}}/2 = \Phi_w^{\text{turb}} \equiv \Phi^{\text{turb}}$. For $\omega > N$, we model the spectrum by an inertial subrange (Corrsin 1963; Lien et al. 1998)

$$\Phi^{\text{turb}}(\omega) = \frac{\beta\varepsilon}{\omega^2} G\left(\frac{\omega}{N}\right) \qquad (N < \omega < \omega_k) \tag{5}$$

$$\Phi^{\text{turb}}(\omega) = 0 \qquad (\omega < N) \tag{6}$$

with a Lagrangian Kolmogorov constant β, which has a value between 1 and 2 (Lien et al. 1998). We use $\beta = 1.8$. For frequencies much larger than a ''large eddy'' frequency, here taken to be N, and much less than a Kolmogorov frequency $\omega_k = (\varepsilon/\nu)^{1/2}$, we set $G = 1$, and the spectrum has the exact inertial subrange form. D'Asaro and Lien (2000) give an analytical expression for G that defines the spectral shape close to N. We assume no turbulent energy for frequencies below N, although this must certainly be an approximation.

Figure 2 shows the evolution of the model $\Phi_w(\omega)$ as a function of internal wave energy. For typical oceanic, that is, Garrett–Munk (GM) energy levels (spectrum A), the internal wave spectrum has far more energy than the turbulence spectrum. This results in a sharp drop in the spectrum near N. This drop is commonly observed, but is particularly sharp when observed from neutrally buoyant floats (Cairns 1975; D'Asaro and Lien 2000; Kunze et al. 1990), that is, for Lagrangian spectra. The ratio $\Delta_{\text{WT}} = \Phi_w^{\text{turb}}(N)/\Phi_w^{\text{iw}}(N)$ will be used to measure the inverse magnitude of the drop; it is small for a large drop. Since the value of ε increases quadratically with wave energy (Gregg 1989; Polzin et al. 1995), Δ_{WT} is proportional to $\Phi_w^{\text{iw}}(N)$. At low energies (spectrum A) Δ_{WT} is small. As the internal wave energy increases (spectrum B), Δ_{WT} also increases until it reaches 1 (spectrum C). At this energy, which will turn out to mark the W–T transition, the drop in the spectral level at N disappears.

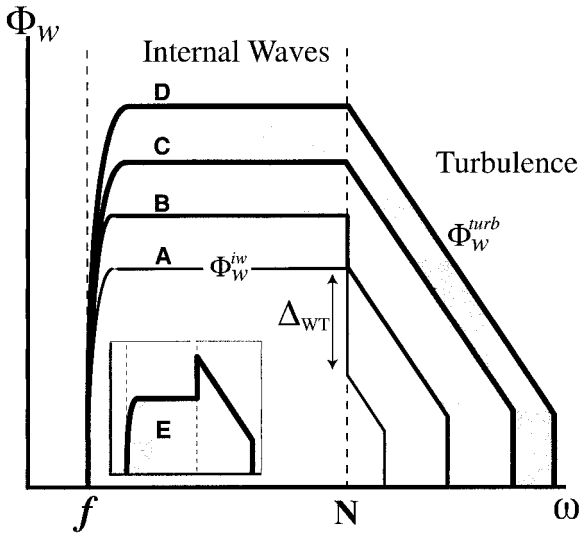

FIG. 2. Evolution of Lagrangian frequency spectrum of vertical velocity with increasing energy. Spectra **A** and **B** are below the W–T transition energy. Spectrum **C** is just at the transition energy. Spectra **D** and **E** are two possible spectra above the transition energy. Spectrum **E** is not observed to occur. The near-discontinuity of the spectrum at frequency N is measured by Δ_{WT}.

If the energy is increased above the W–T transition level, there are two possibilities: Δ_{WT} could continue to increase as shown in spectrum E (Fig. 2, insert), leading to a sharp increase in spectral level at N, or it could remain at unity as shown in spectrum D. D'Asaro and Lien (2000) find no spectra that look like E, but many spectra that look like D. We therefore assume that only spectrum D occurs. D'Asaro and Lien assume this and, using (5) with their analytical expression for G, find

$$\varepsilon = 1.2\beta^{-1}\Phi_w^{iw}N^2 = C_0\,\beta^{-1}\sigma_w^2 N, \tag{7}$$

where $C_0 = 0.6$ is a constant and σ_w^2 is the total vertical velocity variance, including both wave and turbulent components. This expression, valid at or above the W–T transition, shows a linear relationship between energy and dissipation. Thus the W–T transition marks a change from a quadratic to a linear relationship between the energy and turbulent dissipation rate.

The horizontal velocity variance in the frequency spectrum $\Phi_H^{iw}(\omega)$ (Fig. 1) is obtained by integrating (2) while ignoring the small effect of the B factor. For energies well below the W–T transition, the integration extends from f to N. This yields

$$\langle U^2\rangle_L = \int_f^N \Phi_u(\omega)\,d\omega = \phi_0 f\,\sec^{-1}\left(\frac{N}{f}\right) \approx \phi_0 f\pi/2, \tag{8}$$

where the last expression assumes $N \gg f$. At or above the W–T transition, the integration extends from f to about ω_k. Since $\omega_k > N \gg f$ this adds negligible variance.

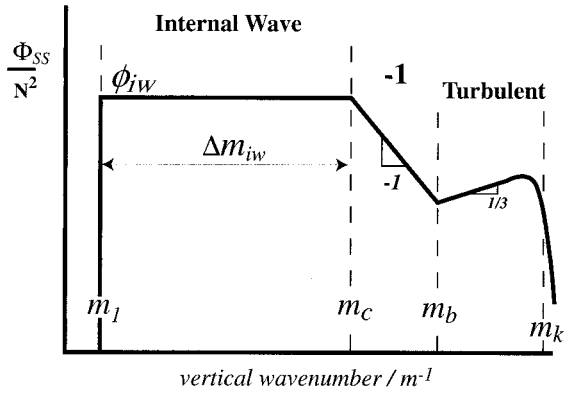

FIG. 3. Model spectra of vertical wavenumber spectrum of shear.

The vertical velocity variance is obtained by integrating $\Phi_w^{iw}(\omega)$ (Fig. 1) to obtain

$$\langle W^2\rangle_L = 2\phi_0\frac{f^2}{N} \tag{9}$$

at or above the W–T transition and half of this well below the W–T transition. The decrease in $\Phi_w^{iw}(\omega)$ for $\omega \approx f$ has been ignored since its effect is small for $N \gg f$.

Using (8) and (9) in (7) yields

$$\varepsilon = \frac{4C_0}{\pi\beta} f\sigma_U^2, \tag{10}$$

where σ_U^2 is the variance of horizontal velocity, again showing a linear relationship between dissipation and energy above the W–T transition. The decay rate of kinetic energy

$$\tau^{-1} \equiv 2\varepsilon/\sigma_U^2 = f\left[\frac{8C_0}{\pi\beta}\right] \tag{11}$$

is constant and approximately equal to $0.8f$.

3. Eulerian wavenumber spectrum

a. Spectral shape

The spectrum, $\Phi_{SS}(m)$ [m s^{-2}] of horizontal shear S [s^{-1}] as a function of vertical wavenumber m [m^{-1}] in the ocean thermocline has been measured by many investigators using vertical profilers (Gregg 1991) that resolve the shear down to dissipation scales. Measurements have been mostly at near-GM energy levels. The basic form, first proposed by Gargett et al. (1981), is shown in Fig. 3. There are three wavenumber bands: a low wavenumber "internal wave" band, a high wavenumber "turbulence" band, and an intermediate "-1" band named for its spectral slope. We will extrapolate this form to energy levels much higher than the GM level using wave–wave interaction theory, and show how it eventually fails.

The low wavenumber band is dominated by internal

waves (Müller et al. 1978). We assume a white normalized shear spectrum, $\Phi_{SS}(m)/N^2$ with a level ϕ_{iw} [m^{-1}], consistent with numerous observations (Gregg et al. 1993; Polzin et al. 1995). Typically, the vertical wavenumber m varies with depth owing to the change of N with depth. This effect can be mostly removed by using a ''WKB-stretched'' wavenumber (Leaman and Sanford 1975), which we use in this analysis. The lower end of the internal wave band is set by the WKB-stretched wavelength of the gravest internal wave mode m_1. For the open ocean, this is set by the thermocline depth; we assume the GM76 value $m_1 = 2\pi/b$ [m^{-1}] with $b = 1300$ m. For the continental shelf, this is set by the water depth; we will use $b = 100$ m.

In the Garrett–Munk spectrum the shear spectral slope changes from white to $+2$ below a vertical mode number j_*. GM76 uses $j_* = 3$. Levine et al. (1997) show evidence that j_* is large for low-energy internal wave fields. Measurements under a storm (D'Asaro 1985) and on the continental shelf (M. Levine 1999, personal communication) suggest that j_* is small for high energy internal wave fields. The data therefore suggest that at energy levels substantially above the GM level, j_* probably falls below 1 and the spectrum is nearly white down to the lowest mode. We therefore ignore the j_* factor in GM76 and retain a white shear spectrum all the way to the lowest mode.

The upper end of the internal wave band is set by the wavenumber m_c, to which we return below. At wavenumbers above m_c the spectral slope changes to -1. At wavenumbers above m_b the spectrum assumes the form of the turbulent ''$-5/3$'' inertial subrange; that is,

$$\Phi_{SS}^{turb} = \alpha_E \varepsilon^{2/3} m^{1/3} \tag{12}$$

out to about the Kolmogorov (viscous) wavenumber $m_k = (\varepsilon/\nu^3)^{1/4}$. The Kolmogorov constant is $\alpha_E = 0.5$, to an accuracy of 10% (Sreenivasan 1995).

b. Internal wave bandwidth

Oceanic observations (Duda and Cox 1989; Sherman and Pinkel 1991; Gregg et al. 1993) suggest an inverse relationship between the wavenumber m_c and the spectral amplitude ϕ_{iw}. Munk (1981) suggests that the value of m_c is set so that the Froude function,

$$\mathrm{Fr}(m) = \int_{m_1}^{m} \frac{\Phi_{SS}(m)}{N^2}\, dm, \tag{13}$$

equals a critical value, i.e., $\mathrm{Fr}(m_c) = \mathrm{Fr}_c$. Polzin et al. (1995) assume this and use $\mathrm{Fr}_c = 0.7$, although values from 0.3 (Sherman and Pinkel 1991) to greater than 1 (Duda and Cox 1989) have also been suggested. For $m_c \gg m_1$ this yields

$$\phi_{iw} m_c = \mathrm{Fr}_c. \tag{14}$$

Using this and the assumed spectral shape yields

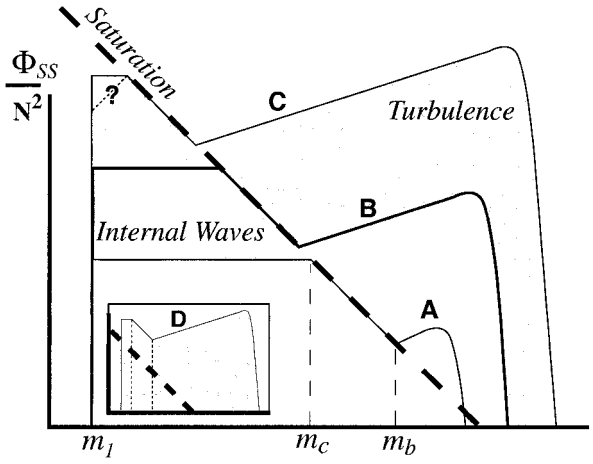

FIG. 4. Evolution of model vertical wavenumber spectra of shear with increasing energy. Spectrum **A** is close to GM energy. With increasing energy the bandwidth of the internal waves shrinks and the bandwidth of turbulence increases, but the spectrum remains tied to the dashed line labeled ''*Saturation.*'' Spectrum **C** is close to the wave-turbulence transition. Spectrum **D** (insert) is not observed.

$$m_b = \left(\frac{\mathrm{Fr}_c}{\alpha_E}\right)^{3/4}\left(\frac{N^3}{\varepsilon}\right)^{1/2} = \left(\frac{\mathrm{Fr}_c}{\alpha_E}\right)^{3/4} m_O, \tag{15}$$

where m_O is the inverse Ozmidov (Ozmidov 1965) scale.

Figure 4 shows the evolution of the vertical wavenumber spectrum with increasing energy assuming that (14) is true. We will measure the internal wave bandwidth by $\Delta m_{iw} = m_1/m_c$. At the GM level (spectrum **A**) Δm_{iw} is small. With increasing energy (spectra **B** and **C**), Δm_{iw} increases, but the ''-1'' region of the spectrum remains on the same curve, the dashed line labeled ''*Saturation.*'' There is considerable experimental support for this result, with very similar scaled spectral levels found both in the ocean (Gargett et al. 1981; Gregg et al. 1993; Winkel 1998) and in the middle atmosphere (Smith et al. 1987; Fritts 1989; Allen and Vincent 1995). In addition, (14) guarentees that m_b is very close to m_O as in (15) so that $1/m_O$ is largest turbulence scale. This is consistent with many oceanographic observations that the overturning (''Thorpe'') and Ozmidov scales are nearly identical (Dillon 1982; Moum 1996).

The model wavenumber spectrum becomes singular as m_c approaches m_1; that is, as Δm_{iw} approaches one. This will mark the W–T transition. In this regime, however, (13) and (14) are no longer equivalent, and the relationship between ϕ_{iw} and m_c becomes uncertain. The obvious assumption is to replace (14) by $\phi_{iw} m_c(1 - \Delta m_{iw}) = \mathrm{Fr}_c$ with the same Fr_c. However, as Δm_{iw} approaches one, this assumption causes the ''-1'' spectral level to rise far above the observed ''*Saturation*'' level and causes m_b to greatly exceed m_O, as shown by spectrum **D** in Fig. 4. This seems to be in disagreement with the observations. We therefore choose to use (14).

There are several possible ways to justify this choice and still maintain the physical simplicity of a critical

value of the Froude function (13). One might suppose that Fr_c decreased as Δm_{iw} approached one, that is, that a narrowband internal wave field might break with less shear than a wide-band one. It seems unlikely that Fr_c could change enough to make this effect important. Alternatively, the internal wave spectral slope might become steeper at high energy, as suggested by the dotted "?" line in Fig. 4. This would produce a peak in the spectrum near m_c and thus decrease the importance of m_1 in the Froude function (13). Both Fritts and VanZandt (1993) and Duda and Cox (1989) find spectra with peaks near m_c, supporting this idea. This would not eliminate the problem, however, just delay it to a larger value of Δm_{iw}. The experimental evidence and theoretical support for (13) is not very strong, and probably less than that in favor of a universal "-1" spectral level, so there is probably no reason to be alarmed if (13) is violated. For the purposes of this paper, it is probably best to view the use of (14) near the W–T transition as an extrapolation of the relations appropriate for the ocean thermocline into a higher energy regime and expect that many of the predicted features will be only qualitatively accurate.

c. Variances

The horizontal velocity variance in the wavenumber spectrum (Fig. 3) is obtained by integrating Φ_{SS}/m^2 while extending the "-1" range to infinity. This yields

$$\langle U^2 \rangle_E = \int_{m_1}^{\infty} \frac{\Phi_{\mathrm{SS}}(m)}{m^2}\, dm = \frac{N^2 \phi_{\mathrm{iw}}}{m_1}\left\{1 - \frac{1}{2}\Delta m_{\mathrm{iw}}\right\}. \quad (16)$$

This ignores a small contribution from the turbulent wavenumber band. The "-1" range contributes $\frac{1}{2}\Delta m_{\mathrm{iw}}$ to the braced expression. Equating (16) and (8) and solving for ϕ_0 yields

$$\phi_0 = \frac{2\phi_{\mathrm{iw}} N^2}{\pi m_1 f}\left\{1 - \frac{1}{2}\Delta m_{\mathrm{iw}}\right\}. \quad (17)$$

We will ignore the braced terms in (16) and (17) since their inclusion leads to much greater algebraic complexity with little gain of insight. Formally, the braced terms can be neglected only well below the W–T transition where Δm_{iw} is small. However, many of the assumptions of our analysis, specifically the assumed Eulerian wavenumber spectral shape, the estimation of m_c, and the parameterization discussed in section 4a, become uncertain near the W–T transition. Different assumptions can change the functional forms of (16) and (17), and subsequent results, in different ways. As in section 3b, the most consistent approach is to view our results as an extrapolation of relations appropriate well below the W–T transition, that is, those with the braced termed ignored, into a higher energy regime.

4. Quantification

a. Dissipation closure

We now compute the energy at which the transitions in the wavenumber and frequency spectra occur. We use the dissipation rate expression of Henyey et al. (1986), as expanded by Henyey (1991), implemented by Polzin et al. (1995), and explained by Winkel (1998). The dissipation rate is computed as the net energy fluxing past vertical wavenumber m_c and is written as the product of three terms:

$$\varepsilon = \underbrace{\frac{\phi_{\mathrm{iw}} N^2}{2m_c^2}\alpha}_{\text{Energy density}}\ \underbrace{(k_H N \mathrm{Fr}_c^{1/2})}_{|dm/dt|}\ \underbrace{\left(\frac{1-r}{1+r}\right)}_{\text{Reflection}}. \quad (18)$$

The first horizontal bracket expresses the energy density at m_c as the product of horizontal kinetic energy density and the ratio α of total to horizontal kinetic energy. The second and third brackets approximate the net rate at which wave packets cross wavenumber m_c under the influence of vertical shear, S. The ray approximation $dm/dt = -k_H S$ is used, where k_H is the horizontal wavenumber. A reflection coefficient r is set to 0.4; S is computed from (13). Combining terms, using single wave approximations for α and k_H/m_c, using (14), and referencing to the GM76 spectrum gives

$$\varepsilon = \varepsilon_0 \frac{m_{c\mathrm{GM}}^2}{m_c^2}\frac{N^2}{N_{\mathrm{GM}}^2}\frac{f}{f_{\mathrm{GM}}}\Gamma = I_0 \Gamma \frac{N^2 f}{m_c^2} = \frac{I_0 \Gamma}{\mathrm{Fr}_c^2} N^2 f \phi_{\mathrm{iw}}^2, \quad (19)$$

where $\varepsilon_0 = 6.7 \times 10^{-10}\ \mathrm{W\,kg^{-1}}$ is a reference dissipation rate for the GM spectrum, $m_{c\mathrm{GM}} = 0.1$ cpm $= 0.628\ \mathrm{m^{-1}}$ is the value of m_c for that spectrum, $f_{\mathrm{GM}} = 6.35 \times 10^{-5}\ \mathrm{s^{-1}}$ is evaluated at 27°N, and $N_{\mathrm{GM}} = 5.24 \times 10^{-3}\ \mathrm{s^{-1}}$. Variations in the energy and wavenumber ratios and the amount of reflection are combined into the Γ factor, which equals 1 for a GM spectrum. The dimensionless factor,

$$I_0 = \frac{\varepsilon_0 m_{c\mathrm{GM}}^2}{N_{\mathrm{GM}}^2 f_{\mathrm{GM}}} = 0.15, \quad (20)$$

frees the analysis from the arbitrary "GM" scales, which have plagued the literature for decades. Equation (19) is the same as Winkel's (1998) equation (5.7) and Polzin et al.'s 1995 equation (11) at 27°N. Both authors find it to be accurate to about a factor of 2 if the variations in Γ are included.

The dissipation rate in (19) is proportional to the internal wave spectral level squared, ϕ_{iw}^2. Substituting (16), (8), (9), and defining $\sigma_U^2 = \langle U^2 \rangle$ and $\sigma_W^2 = \langle W^2 \rangle$ as the horizontal and vertical velocity variances, respectively, and ignoring braced terms, we find

$$\varepsilon = \frac{I_0 \Gamma}{\mathrm{Fr}_c^2} f \frac{m_1^2}{N^2} \sigma_U^4. \quad (21)$$

The dissipation rate is proportional to the kinetic energy squared. The decay rate of kinetic energy

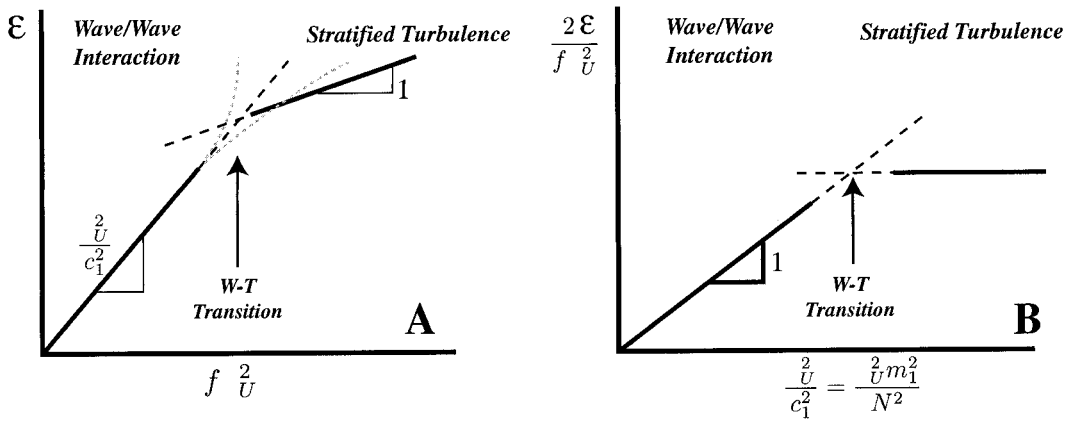

FIG. 5. The W–T transition energy defined as the intersection of the wave–wave interaction and stratified turbulence model predictions of ε as a function of σ_U^2. The coordinates are log–log. Gray-dashed lines show possible extrapolation errors near the transition: (a) dimensional and (b) nondimensional.

$$\tau^{-1} \equiv \frac{2\varepsilon}{\sigma_U^2} = f\left[\frac{2I_0\Gamma}{\mathrm{Fr}_c^2}\right]\left(\frac{\sigma_U}{c_1}\right)^2, \tag{22}$$

where $c_1 \equiv N/m_1$ is approximately the phase speed of the lowest mode. The bracketed expression is close to unity (0.61), and we have neglected the small contribution of vertical kinetic energy for $N \gg f$ as well as the braced term in (16). The decay rate is proportional to the nonlinearity of the lowest mode, given by the ratio of the typical horizontal velocity to c_1.

b. The W–T transition

We now compute the kinetic energy of the W–T transition in three different ways and show that they are nearly equivalent. Equation (21) predicts a quadratic relationship between ε and kinetic energy σ_U^2. Equation (10) predicts a linear relationship. The intersection of these two relationships, one valid at low energy and one valid at high energy, defines the first estimate of the W–T transition energy (Fig. 5a),

$$\sigma_U|_{\mathrm{WT}} = c_1\left[\frac{4C_0\mathrm{Fr}_c^2}{\beta\pi I_0\Gamma}\right]^{1/2} \equiv (2C_0W_0)^{1/2}c_1 \approx 1.1c_1, \tag{23}$$

where $W_0 = 2\mathrm{Fr}_c^2/\beta\pi I_0\Gamma \approx 1.1$ is a dimensionless parameter.

The second estimate assumes $\Delta_{\mathrm{WT}} = 1$ (Fig. 1) at the W–T transition. Combining (5) and (4) yields $\Delta_{\mathrm{WT}} = \beta\varepsilon/\phi_0 f^2$. Substituting for ε, using (21) and (8) for σ_U^2, yields

$$\Delta_{\mathrm{WT}} = W_0^{-1}\frac{\sigma_U^2}{c_1^2}. \tag{24}$$

Setting $\Delta_{\mathrm{WT}} = 1$ gives $\sigma_U|_{\mathrm{WT}} = 1.1c_1$.

The third estimate assumes $\Delta m_{\mathrm{iw}} = 1$ (Fig. 4) at the W–T transition. Combining (16) and (14) yields

$$\sigma_U^2|_{\mathrm{WT}} = c_1^2\mathrm{Fr}_c\Delta m_{\mathrm{iw}}. \tag{25}$$

Setting $\Delta m_{\mathrm{iw}} = 1$ yields $\sigma_U|_{\mathrm{WT}} = 0.6c_1$, where the braced factors have again been ignored.

The three estimates yield results identical within the errors in the various coefficients and the substantial theoretical uncertainties described in section 3. Thus at the W–T transition $\Delta_{\mathrm{WT}} = 1$, that is, the turbulent and internal wave spectra merge in the Lagrangian frequency spectrum; $\Delta m_{\mathrm{iw}} \approx 1$, that is, the internal wave bandwidth in the Eulerian wavenumber spectrum becomes small; and $\sigma_U \approx c_1$, that is, the rms velocity equals the phase velocity of the lowest mode; and the linear and quadratic parameterizations of ε converge. This is the main result of the paper.

These conclusions result from the extrapolation of results at small σ_U^2 into a regime where they may not be valid. This is schematically illustrated in Fig. 5a by the dark dashed lines showing the extrapolation and the gray dashed lines showing possible corrections to the extrapolation near the W–T transition. Although it is clear that a transition must occur, details near the transition are not captured by our analysis.

c. Physics

The W–T transition, as computed here, marks the energy level where the basic assumptions of GM-based wave–wave interaction theories fail. At open ocean energy levels and water depths almost all of the energy is in the internal wave wavenumber band and can be reasonably represented by the sum of internal wave modes. The transfer of energy from these scales to the smaller-scale turbulence is due to wave–wave interactions. Henyey et al.'s (1986) model of this (19) assumes the interaction of individual ''test'' waves with the ''internal wave'' band of wavenumbers in Fig. 3. At the W–T transition, m_c and m_1 become nearly equal, this band becomes small, and the wave–wave interaction theory becomes ill posed. In addition, the Richardson number of the lowest wavenumbers, that is, m_1, becomes order

1 on average, and their velocity approaches the fastest wave phase speed. Statistical fluctuations will reduce the Richardson number to below critical (¼) in places, resulting in localized shear instability of the large-scale motions. The large-scale motions thus become locally unstable to shear instability and can directly transfer energy to turbulence. Alternatively, the large-scale waves will start to break since their velocity is comparable to their phase speed. This is the physics of stratified turbulence. Thus, the W–T transition marks a change from energy transfer controlled by wave–wave interaction to that controlled by instability and turbulence.

d. The transition energy level

The spectral level of the W–T transition relative to the GM level can be predicted by finding the internal wave spectral level that sets $m_c = m_1$ in (14):

$$\frac{\phi_{\text{trans}}}{\phi_{\text{GM}}} = \frac{m_{c\text{GM}}}{m_1}, \tag{26}$$

where ϕ_{GM} is the value of ϕ_{iw} for the GM spectrum. The kinetic energy at the transition, whether calculationed by (23), (24), or (25), is approximately

$$\text{KE}_{\text{trans}} = \frac{1}{2}c_1^2 = \frac{1}{2}\frac{N^2}{m_1^2}. \tag{27}$$

According to (11), the turbulent kinetic dissipation rate is proportional to the kinetic energy times τ^{-1}, so

$$\varepsilon_{\text{trans}} = f\text{KE}_{\text{trans}} \tag{28}$$

since $\tau^{-1} \approx f$ at the transition.

For deep ocean depths ($m_1 = 2\pi/1300$ m, $m_{c\text{GM}} = 2\pi/10$ m) (26) predicts the W–T transition at 130 times the GM spectral level, (27) predicts an internal wave horizontal kinetic energy at the transition of (0.7 m $s^{-1})^2$, and (28) predicts $\varepsilon = 3 \times 10^{-5}$ W kg^{-1} at the transition. Values of ε this large are rarely, if ever, observed in the open ocean thermocline (Gregg 1998). It appears to remain almost always below the W–T transition.

In shallow water, the low modes are excluded, and there is much more shear per unit kinetic energy. Consequently, the W–T transition occurs at lower energy. Equivalently, the lowest mode phase speed c_1 is lower for the same (assumed constant) stratification, so lower water velocities are needed match c_1. In 100 m of water, (26) predicts the W–T transition at 10 times the GM spectral level, (27) predicts an internal wave horizontal kinetic energy at the transition of (0.06 m $s^{-1})^2$, and (28) predicts $\varepsilon = 2 \times 10^{-7}$ W kg^{-1} at the transition. Moum and Nash (1999, personal communication) report ε values much larger than this over rough topography on the Oregon shelf. Gregg et al. (1999) report substantially larger values on the shelf near Monterey Bay. The flows in these locations are energetic enough to be clearly above the W–T transition. Flows at other locations on the shelf are clearly less energetic and lie below the transition.

5. Parameterizations

a. Quadratic

There is ample evidence for quadratic scaling of ε with energy in the ocean thermocline (Gregg 1989; Polzin et al. 1995; Winkel 1998) and considerable theoretical justification (Winters and D'Asaro 1997; Müller et al. 1986). In this regime the Richardson number is above critical and the flow is mostly laminar. In places, the Richardson number falls below critical, creating localized turbulence and mixing. The frequency and intensity of these mixing events are controlled by the supply of energy from the wave–wave interactions at larger scale (Polzin 1996; Pinkel and Anderson 1997), which therefore control the overall rate of mixing.

b. Linear

In the high energy, stratified turbulence regime, we predict a dissipation rate linearly proportional to the energy

$$\varepsilon = C\sigma_w^2 N. \tag{29}$$

We estimate $C = C_0/\beta = 0.3$–0.6 (7); the uncertainly is set primarily by the uncertainty in β. Parameterizations of this form are common in the literature. Weinstock (1981) suggests $C = 0.4$–0.5 as a good predictor of dissipation in the stratosphere. Moum (1996) finds $C = 0.73 \pm 0.06$ for turbulent patches in the ocean thermocline. His measurement of σ_w^2 is biased low by an instrumental high-pass filter, consistent with an estimate of C that is biased high. Observations in the upper equatorial Pacific, a region of high mean shear and turbulence, show strong linear relationships between the turbulent dissipation rate and several measures of internal wave energy (wave isotherm displacement, wave slope, and wave potential energy) (Moum et al. 1992; Lien et al. 1996). We have reanalyzed the data presented by Lien et al. (1996) and find a strong linear relationship ($r^2 = 0.64$) between σ_w^2, measured from the isothermal displacement rate, and ε. The estimated $C = 0.1$. This measurement of σ_w^2 is biased high by temperature fluctuations due to horizontal advection, consistent with a value of C that is biased low.

c. Stratified turbulence models

The model presented here yields results similar to those from the high-stratification, low-energy limit of commonly used two-equation stratified turbulence models. We discuss the model presented by Burchard et al. (1998, henceforth BPR), which is very close to that of Mellor and Yamada (1982) as modified by Galperin et

al. (1988, henceforth G88). The low-energy, high-stratification limit of the model is set by a maximum value of 0.56 for $\alpha_N = L^2N^2/k$ [BPR Eq. (15)]. Here $k = \frac{1}{2}(\sigma_u^2 + \sigma_w^2)$ is the turbulent kinetic energy and $L = 0.56^3k^{3/2}/\varepsilon$ is the master turbulence length scale [BPR Eq. (11)]. Combining these yields

$$L = 1.6(\varepsilon/N^3)^{1/2} \tag{30}$$

$$\varepsilon = 0.212kN \tag{31}$$

[BPR Eq. (16)]. Combining these with BPR's Eq. (14) and Eq. (30) yields the following expression for the turbulent diffusivity of mass:

$$K_\rho = \gamma\varepsilon/N^2; \qquad \gamma = 0.24. \tag{32}$$

Equations (30) and (32) are well established in the ocean mixing literature. Equation (30) states that the outer scale of the turbulence is the Ozmidov scale (Dillon 1982), or m_b^{-1}, the upper end of the ''-1'' wavenumber band in our model. Equation (32) is the Osborn (1980) expression, which forms the basis for dissipation-based estimates of ocean mixing rates.

Equation (31) uses k, the total kinetic energy, rather than its vertical component $\sigma_w^2/2$ as in (29). We define $A \equiv \sigma_w^2/k$ as a measure of the anisotropy of the flow so that (31) predicts $C = 0.212/A$. For an isotropic flow, $A = 0.66$ and $C = 0.32$. G88's Eq. (31) predicts $A = 0.3$ in the high stratification limit, yielding $C = 0.71$. These numbers are comparable to those predicted by (7).

Thus the high stratification limit of the BPR model reproduces many of the basic equations of oceanic mixing. Despite this, there are fundamental conceptual differences between these stratified turbulence models and the model presented here. The stratified turbulence models claim to represent only the ''turbulent'' velocity fluctuations. Thus k in (31) is the turbulent kinetic energy. Here, we propose that much of the energy and all of the anisotropy in stratified turbulence is due to its internal wave component, as is discussed in more detail by D'Asaro and Lien (2000) and Hanazaki and Hunt (1996). Internal waves, in this view, are an intrinsic part of stratified turbulence. Thus σ_w^2 in (7) includes all of the vertical velocity variance. The anisotropy of the flow depends primarily on the low-frequency cutoff of the Lagrangian frequency spectrum not, as in G88, on the parameter α_N. For the oceanic spectra, (8) and (9) imply $A \approx 4f/\pi N$, which will usually be far below the G88 minimum value of 0.3. The observation that both the high-energy limit of the model presented here and the low-energy limit of BPR yield similar parameterizations [Eqs. (30), (31), (32)] suggests that a hybrid model, combining appropriate aspects of each, may be possible.

BPR find that their model greatly underpredicts ε in the stratified thermocline. Their solution is to continue to use (31), but to set an arbitrary lower limit $k > k_{\min}^2$ in order to include ''internal wave breaking.'' We suggest that the problem is more fundamental. Their model, tuned to work above the W–T transition, fails to work below it. We suggest that, close to the transition, (29) will be superior to (31). Below the transition, (19) should be used along with model components that track the generation, propagation, and interactions of internal waves.

d. N scaling of diffusivity

We have emphasized how the dynamics of a stratified flow vary with energy. Alternatively, one can view the decay rate of kinetic energy as a function of stratification at fixed energy, as shown in Fig. 5b. Below the W–T transition a ''$+2$'' slope is found (22); above the transition the decay rate is constant (11).

The diapycnal diffusivity of mass due to internal-wave-driven turbulence is often computed from (32) using a mixing efficiency γ of about 0.2 (Ivey and Imberger 1991). For energies below the W–T transition, (19) leads to a diffusivity independent of N and proportional to the internal wave spectral level ϕ_{iw} squared. For energies above the W–T transition, (7) leads to a diffusivity proportional to $\sigma_w^2N^{-1}$. Gargett (1984) showed that seasonally averaged diffusivities in lakes and fjords scaled as N^{-1} and proposed this scaling for the ocean interior. Subsequent measurements have showed this to be inappropriate for the ocean. Fjords are usually mixed by vigorous turbulence at a sill (D'Asaro and Lien 2000; Farmer and Freeland 1983), while lakes are often mixed by the rapid breakdown of intermittent wind-generated seiches (Imberger 1994). We suggest that Gargett's (1984) scaling is appropriate for fjords and lakes because they are mixed by strong turbulence above the W–T transition and inappropriate for the open ocean because it is mixed by motions below the W–T transition.

6. Summary and discussion

We hypothesize the existence of two distinct dynamical regimes for mixing in stratified flows. At low energies, flow evolution is controlled by interactions between internal wave modes. At high energies, flow evolution is controlled by instabilities of the wave modes. The ''wave–turbulence'' transition separating these regimes is marked by

- an rms velocity approximately equal to the phase speed of the lowest internal wave mode
- the merging of the internal wave and turbulence spectra near Lagrangian frequency N (Fig. 2)
- the decrease of the large-scale Richardson number to near one
- the reduction of the internal wave vertical wavenumber bandwidth to a small value (Fig. 4)
- a change from a quadratic relationship between wave energy and dissipation rate at low energies (19) to a linear relationship at high energies (7).

Existing parameterizations of the Lagrangian and Eulerian wavenumber spectral shapes (Figs. 1 and 3), combined with the Polzin et al. (1995) parameterization of dissipation rate (19), predict that all of the above will occur at nearly the same energy. The shape of the Lagrangian and Eulerian spectra (Figs. 2 and 4) may be a useful diagnostic as to whether a given flow is above or below the W–T transition.

The W–T transition is predicted to occur at a lower average dissipation rate and internal wave shear, but similar energy density, in shallow water than in deep water [Eqs. (26), (27), (28)]. The open ocean thermocline is likely to remain below the transition, but flow on the continental shelves may often rise above it. The upper atmosphere appears to be close to the transition, judging from the small range of wavenumbers below m_c. Turbulence parameterization schemes that ignore internal waves will be accurate only for energies above the transition.

The present analysis, although aimed mostly at oceanic applications, should also be relevant to other stratified flows. The most obvious obstacle is the presence of the Coriolis frequency f in many of the expressions. This appears, first, because the internal wave energy in the ocean is dominated by motions near f. Expressions (2) and (4) describing energy spectra thus contain f. Second, the internal wave dissipation closure (18) depends most fundamentally on the horizontal wavenumber, k_H, parameterized in (19) by the vertical wavenumber m times the aspect ratio of the flow, which is proportional to f/N. In neither case is f fundamental to the analysis, and a theory in which f did not appear could be formulated. Henyey (1991) gives a short description of how to proceed.

Although the analysis above has enabled us to sketch the nature of the W–T transition some features remain unsatisfactory. In particular, the results are sensitive to low-mode, low-frequency energy that dominates the internal wave energy spectrum. It seems far more likely that the high modes, that is, the shear rather than the energy, are important, but we do not have measurements of their frequency spectra. The analysis would thus be more satisfactory if it were formulated using Lagrangian and Eulerian spectra of either shear or vertical velocity. Similarly, the analysis ignores zero frequency motions, although any mean shear must be important if sufficiently large. This may explain the absence of ''vortical modes'' (Müller et al. 1986) in the formulation. Furthermore, peaks in energy at frequencies near N are often observed; these could significantly modify the results. The analysis depends heavily on assumptions about the ''-1'' wavenumber range in the shear spectrum. It is unsettling that the dynamical nature of this region remains unresolved (Holloway 1983; Hines 1991; Eckermann 1999; Gardner 1996; Pinkel and Anderson 1997). Finally, we have been unable to formulate a satisfactory theory near the W–T transition, as shown by the neglect of ''braced'' expressions throughout the analysis. Our results are bold extrapolations from above and below the transition. There is a clear need for measurements, particularly of vertical wavenumber spectra near and above the transition, to test the various assumptions required here.

REFERENCES

Allen, S. J., and R. A. Vincent, 1995: Gravity wave activity in the lower atmosphere: Seasonal and latitudinal variations. *J. Geophys. Res.,* **100,** 1327–1350.

Burchard, H., O. Petersen, and T. P. Rippeth, 1998: Comparing the performance of the Mellor–Yamada and the k–ε two-equation turbulence models. *J. Geophys. Res.,* **103** (C5), 10 543–10 554.

Cairns, J., 1975: Internal wave measurements from a midwater float. *J. Geophys. Res.,* **80** (3), 299–306.

——, and G. O. Williams, 1976: Internal wave observations from a midwater float, 2. *J. Geophys. Res.,* **81,** 1943–1950.

Calman, J., 1978: On the interpretation of ocean current spectra. II: Testing dynamical hypotheses. *J. Phys. Oceanogr.,* **8,** 644–652.

Corrsin, S., 1963: Estimates of the relations between Eulerian and Lagrangian scales in large Reynolds number turbulence. *J. Atmos. Sci.,* **20,** 115–199.

D'Asaro, E., 1985: Upper ocean temperature structure, inertial currents and Richardson numbers during strong meteorological forcing. *J. Phys. Oceanogr.,* **15,** 943–962.

——, and R. C. Lien, 2000: Lagrangian measurements of waves and turbulence in stratified flows. *J. Phys. Oceanogr.,* **30,** 641–655.

Dillon, T. M., 1982: Vertical overturns: A comparison of Thorpe and Ozmidov length scales. *J. Geophys. Res.,* **87,** 9601–9613.

Duda, T. F., and C. S. Cox, 1989: Vertical wave number spectra of velocity and shear at small internal wave scales. *J. Geophys. Res.,* **94,** 939–950.

Eckermann, S. D., 1999: Isentropic advection by gravity waves: Quasi-universal m^3 vertical wavenumber spectra near the onset of instability. *Geophys. Res. Lett.,* **26,** 201–204.

Farmer, D. M., and H. J. Freeland, 1983: The physical oceanography of fjords. *Progress in Oceanography,* Vol. 12, Pergamon, 147–220.

Fofonoff, N. P., 1969: Spectral characteristics of internal waves in the ocean. *Deep-Sea Res.,* **16,** 59–71.

Fritts, D. C., 1989: A review of gravity wave saturation processes, effects and variability in the middle atmosphere. *Pure Appl. Geophys.,* **130,** 343–371.

——, and T. E. VanZandt, 1993: Spectral estimates of gravity wave energy and momentum fluxes. Part I: Energy dissipation, acceleration and constraints. *J. Atmos. Sci.,* **50,** 3685–3694.

Galperin, B., L. H. Kantha, S. Hassid, and A. Rosati, 1988: A quasi-equilibrium turbulent energy model for geophysical flows. *J. Atmos. Sci.,* **45,** 55–62.

Gardner, C. S., 1996: Testing theories of atmospheric gravity wave saturation and dissipation in the middle atmosphere. *J. Atmos. Terr. Phys.,* **58,** 1575–1589.

Gargett, A. E., 1984: Vertical eddy diffusivity in the ocean interior. *J. Mar. Res.,* **42,** 359–393.

——, P. J. Hendricks, T. B. Sanford, T. R. Osborn, and A. J. Williams III, 1981: A composite spectrum of vertical shear in the upper ocean. *J. Phys. Oceanogr.,* **11,** 1258–1271.

Garrett, C. J. R., and W. H. Munk, 1975: Space–time scales of internal waves: A progress report. *Annu. Rev. Fluid Mech.,* **11,** 339–369.

Gregg, M. C., 1989: Scaling turbulent dissipation in the thermocline. *J. Geophys. Res.,* **94,** 9686–9698.

——, 1991: The study of mixing in the ocean: A brief history. *Oceanography,* **4,** 39–45.

——, 1998: Estimation and geography of diapycnal mixing in the stratified ocean. *Physical Processes in Lakes and Oceans,* Coastal and Estuarine Studies, Vol. 54, Amer. Geophys. Union, 305–338.

——, and E. Kunze, 1991: Shear and strain in Santa Monica Basin. *J. Geophys. Res.,* **96,** 16 709–16 719.
——, D. P. Winkel, and T. B. Sanford, 1993: Varieties of fully resolved spectra of vertical shear. *J. Phys. Oceanogr.,* **23,** 124–141.
——, ——, J. A. MacKinnon, and R. C. Lien, 1999: Mixing over shelves and slopes. *Internal Wave Modelling, Proc. 'Aha Huliko'a Hawaiian Winter Workshop,* P. Müller and D. Henderson, Eds., Honolulu, HI, Hawaii Institute of Geophysics, 35–42.
Hanazaki, H., and J. C. R. Hunt, 1996: Linear processes in unsteady stably stratified turbulence. *J. Fluid Mech.,* **318,** 303–337.
Henyey, F., 1989: Why eddy diffusivity doesn't work. *Internal Gravity Waves and Small-Scale Turbulence, Proc. 'Aha Huliko'a Hawaiian Winter Workshop,* P. Müller and D. Henderson, Eds., Honolulu, HI, Hawaii Institute of Geophysics, 245–250.
——, 1991: Scaling of internal wave predictions for ε. *Internal Gravity Waves and Small-Scale Turbulence, Proc. 'Aha Huliko'a Hawaiian Winter Workshop,* P. Müller and D. Henderson, Eds., Honolulu, HI, Hawaii Institute of Geophysics, 233–236.
——, J. Wright, and S. M. Flatté, 1986: Energy and action flow through the internal wave field: An Eikonal approach. *J. Geophys. Res.,* **91,** 8487–8495.
Hines, C. O., 1991: The saturation of gravity waves in the middle atmosphere. Part I: Critique of linear-instability theory. *J. Atmos. Sci.,* **48,** 1348–1359.
Holloway, G., 1983: A conjecture relating oceanic internal waves and small-scale processes. *Atmos.–Ocean,* **21,** 107–122.
Imberger, J., 1994: Transport processes in lakes: A review. *Limnology Now: A Paradigm of Planetary Problems,* R. Margalef, Ed., Elsevier-Science, 99–193.
Ivey, G. M., and J. Imberger, 1991: On the nature of turbulence in a stratified fluid, Part I: The energetics of mixing. *J. Phys. Oceanogr.,* **21,** 650–658.
Kunze, E., M. G. Briscoe, and A. J. Williams III, 1990: Interpreting shear and strain fine structure from a neutrally buoyant float. *J. Geophys. Res.,* **95** (C10), 18 111–18 125.
Leaman, K. D., and T. B. Sanford, 1975: Vertical energy propagation of inertial waves: A vector spectral analysis of velocity profiles. *J. Geophys. Res.,* **80,** 1975–1978.
Levine, M. D., L. Padman, R. D. Muench, and J. H. Morison, 1997: Internal waves and tides in the western Weddell Sea: Observations from Ice Station Weddell. *J. Geophys. Res.,* **102** (C1), 1073–1089.
Lien, R. C., M. J. McPhaden, and M. C. Gregg, 1996: High-frequency internal waves at 0°, 140°W and their possible relationship to deep-cycle turbulence. *J. Phys. Oceanogr.,* **26,** 581–600.
——, E. A. D'Asaro, and G. T. Dairiki, 1998: Lagrangian frequency spectra of vertical velocity and vorticity in high-Reynolds number oceanic turbulence. *J. Fluid Mech.,* **362,** 177–198.
Luyten, P., E. Deleersnijder, J. Ozer, and K. Ruddick, 1996: Presentation of a family of turbulence closure models for stratified shallow water flows and preliminary application to the Rhine outflow region. *Contin. Shelf Res.,* **16,** 101–130.
Mellor, G. L., and T. Yamada, 1982: Development of a turbulence closure model for geophysical fluid problems. *Rev. Geophys. Space Phys.,* **20,** 851–875.
Moum, J. N., 1996: Energy-containing scales of turbulence in the ocean thermocline. *J. Geophys. Res.,* **101** (C6), 14 095–14 109.
——, D. Herbert, C. A. Paulson, and D. R. Caldwell, 1992: Turbulence and internal waves at the equator. Part I: Statistics from towed thermistors and a microstructure profiler. *J. Phys. Oceanogr.,* **22,** 1330–1345.
Müller, P., D. J. Olbers, and J. Willebrand, 1978: The IWEX spectrum. *J. Geophys. Res.,* **83,** 479–500.
——, G. Holloway, F. Henyey, and N. Pomphrey, 1986: Nonlinear interactions among internal gravity waves. *Rev. Geophys.,* **24,** 493–536.
Munk, W. H., 1981: Internal waves and small-scale processes. *Evolution of Physical Oceanography,* C. Wunsch, Ed., The MIT Press, 264–291.
Osborn, T. R., 1980: Estimates of the local rate of vertical diffusion from dissipation measurements. *J. Phys. Oceanogr.,* **10,** 83–89.
Ozmidov, R. V., 1965: On the turbulent exchange in a stably stratified ocean. *Izv. Acad. Sci. USSR, Atmos. Oceanic Phys.,* **1,** 853–860.
Pinkel, R., and S. Anderson, 1997: Shear, strain and Richardson number variations in the thermocline. Part II: Modeling mixing. *J. Phys. Oceanogr.,* **27,** 282–290.
Polzin, K., 1996: Statistics of the Richardson number: Mixing models and finestructure. *J. Phys. Oceanogr.,* **26,** 1409–1425.
——, J. Toole, and R. Schmitt, 1995: Finescale parameterizations of turbulent dissipation. *J. Phys. Oceanogr.,* **25,** 306–328.
Sherman, J., and R. Pinkel, 1991: Estimates of the vertical wavenumber-frequency spectrum of vertical shear and strain. *J. Phys. Oceanogr.,* **21,** 292–303.
Simpson, J. H., W. R. Crawford, T. P. Rippeth, A. R. Campbell, and J. V. S. Cheok, 1996: The vertical structure of turbulent dissipation in shelf seas. *J. Phys. Oceanogr.,* **26,** 1579–1590.
Smith, S. A., D. C. Fritts, and T. E. VanZandt, 1987: Evidence for a saturated spectrum of atmospheric gravity waves. *J. Atmos. Sci.,* **44,** 1404–1410.
Sreenivasan, K., 1995: On the universality of the Kolmogorov constant. *Phys. Fluids,* **7,** 2778–2784.
Weinstock, J., 1981: Energy dissipation rates of turbulence in the stable free atmosphere. *J. Atmos. Sci.,* **38,** 880–883.
Winkel, D., 1998: Influences of mean shear in the Florida Current on turbulent production by internal waves. Ph.D. thesis, University of Washington, 138 pp.
Winters, K. E., and E. A. D'Asaro, 1997: Direct simulation of internal wave energy transfer. *J. Phys. Oceanogr.,* **27,** 1937–1945.